Magnetically active pNIPAM nanosystems as temperature-sensitive biocompatible structures for controlled drug delivery

Beatriz Garcia-Pinel , Alicia Ortega-Rodríguez , Cristina Porras-Alcalá , Laura Cabeza , Rafael Contreras-Cáceres , Raul Ortiz , Amelia Díaz , Ana Moscoso , Francisco Sarabia , José Prados , Juan M. López-Romero & Consolación Melguizo

Taylor & Francis
Taylor & Francis Group

Magnetically active pNIPAM nanosystems as temperature-sensitive biocompatible structures for controlled drug delivery
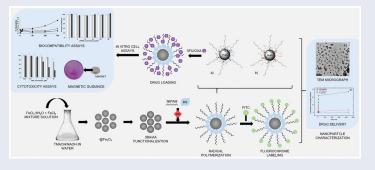
Beatriz Garcia-Pinel[a,b,c], Alicia Ortega-Rodríguez[d], Cristina Porras-Alcalá[d], Laura Cabeza[a,b,c], Rafael Contreras-Cáceres[e], Raul Ortiz[a,b,c], Amelia Díaz[d], Ana Moscoso[d], Francisco Sarabia[d], José Prados[a,b,c], Juan M. López-Romero[d]* and Consolación Melguizo[a,b,c]*

[a]Institute of Biopathology and Regenerative Medicine (IBIMER), Center of Biomedical Research (CIBM), University of Granada, Granada, Spain; [b]Department of Anatomy and Embriology, Faculty of Medicine, University of Granada, Granada, Spain; [c]Instituto de Investigación Biosanitaria ibs.GRANADA, Granada, Spain; [d]Department of Organic Chemistry, Faculty of Sciences, University of Málaga, Málaga, Spain; [e]Department of Chemistry in Pharmaceutical Science, Faculty of Pharmacy, Complutense University of Madrid, Madrid, Spain

ABSTRACT

Here, temperature-sensitive hybrid poly(N-isopropylacrylamide) (pNIPAM) nanosystems with magnetic response are synthesised and investigated for controlled release of 5-fluorouracil (5FU) and oxaliplatin (OXA). Initially, magnetic nanoparticles (@Fe_3O_4) are synthesised by co-precipitation approach and functionalised with acrylic acid (AA), 3-butenoic acid (3BA) or allylamine (AL) as comonomers. The thermo-responsive polymer is grown by free radical polymerisation using N-isopropylacrylamide (NIPAM) as monomer, N,N'-methylenbisacrylamide (BIS) as cross-linker, and 2,2'-azobis(2-methylpropionamidene) (V50) as initiator. We evaluate particle morphology by transmission electron microscopy (TEM) and particle size and surface charge by dynamic light scattering (DLS) and Z-potential (ZP) measurements. These magnetically active pNIPAM@ nanoformulations are loaded with 5-fluorouracil (5FU) and oxaliplatin (OXA) to determine loading efficiency, drug content and release as well as the cytotoxicity against T-84 colon cancer cells. Our results show high biocompatibility of pNIPAM nanoformulations using human blood cells and cultured cells. Interestingly, the pNIPAM@Fe_3O_4-3BA + 5FU nanoformulation significantly reduces the growth of T-84 cells (57% relative inhibition of proliferation). Indeed, pNIPAM-co-AL@Fe_3O_4-AA nanosystems produce a slight migration of HCT15 cells in suspension in the presence of an external magnetic field. Therefore, the obtained hybrid nanoparticles can be applied as a promising biocompatible nanoplatform for the delivery of 5FU and OXA in the improvement of colon cancer treatments.

GRAPHICAL ABSTRACT

Introduction

Colorectal cancer is one of the most common causes of cancer worldwide (10.2% of all the cases of cancer diagnosed in 2018) and shows an alarming mortality (9.2%) only surpassed by lung cancer (18.4%) [1]. The chemotherapeutic treatment, mostly administered in stage II or III or higher [2], includes 5-Fluorouracil (5FU) as the first-line drug which is often used in combination with other antitumor drugs such as oxaliplatin (OXA) (FOLFOX) [2,3]. 5FU is an analog of pyrimidine that is able to inhibit the enzyme thymidylate synthase [4,5] and OXA is an antitumor drug of platinum family that has a synergistic effect with fluoropyrimidines [6,7]. However, the

non-specificity of both 5-FU and OXA, the rapid metabolisation and excretion of 5FU as well as the induction of peripheral neuropathy by OXA, among others, limit their use in colorectal cancer treatment [8,9]. In this context, the association of cytotoxic drugs to nanoplatforms is a new approach to improve their antitumor efficiency to reduce their adverse effects [10].

During the last years, nanogels have attracted considerable attention concerning cytotoxic drug transport. The principal advantage of these cross-linked colloidal systems are the high particle stability, a tuneable degree of flexibility and most importantly a high sensitivity to certain external stimuli, such as temperature [11], pH [12], solvent nature [13], ionic strength [14] or electric field [15]. In this context, pNIPAM, which is the most used stimuli-responsive polymer in nanomedicine, has the advantage to collapses at a temperature near the human body. This microgel undergoes a reversible volume phase transition (VPT) in response to temperature with a lower critical solution temperature (LCST) (around $32\,^\circ$C in water). This means that the microgel swells by the incorporation of solvent molecules (e.g. water), due to the formation of H-bonds between water and acrylamide groups. On contrary, above the LCST, the water molecules are expelled due to the breakage of H-bonds that causes the microgel to collapse due to the high hydrophobicity of the methylene groups. During the last years, pNIPAM has been used to accumulate and release certain types of chemotherapeutic drugs. Specifically for drug delivery, Rejinold et al. encapsulated 5FU into pNIPAM nanogels (in the presence of fibrinogen) increasing breast cancer cells apoptosis [16]. 5FU was also incorporated into poly(p-nitrophenol acrylate)-co-(N-isopropylacrylamide) to obtain nanohydrogels with different drug loading. These systems presented low cytotoxicity but unfortunately, it incremented with the hydrogel concentration [17]. More recently, pNIPAM-MAPOSS hybrid microgels in the presence of PEG was used as a drug carrier for 5FU. These authors were able to adjust the pore size by controlling the amount of PEG [18]. Concerning OXA, Patil et al. synthesised biodegradable OXA-loaded chitosan-graft-poly-N-isopropylacrylamide and Peng et al. fabricated a dual responsive nanogel for OXA encapsulation, which was loaded *via* conjugation with the carboxylic groups [19,20]. These authors found that the OXA was released much faster at a more acidic environment. In addition, two different methods were used for the synthesis of chitosan-g-poly(N-isopropylacrylamide) (Cs-g-pNIPAM) co-polymer to developed highly loaded pH- and thermo-responsive nanoparticles (NPs) for tumour-specific OXA delivery. More recently, higher OXA loading was obtained by using a self-assembly method, compared with a direct loading method [21]. However, during the last years, hybrid nanostructures composed by magnetic NPs encapsulated by pNIPAM have improved drug delivery efficiencies. The improvement in including magnetic nanoparticles is that these hybrid microgels are able to respond to an external magnetic field, thus improving transport activity. Moreover, these colloidal systems also exhibit an amphiphilic behaviour with a hydrophilic nature and good dispersibility in water below LCST, while show a hydrophobic nature

above LCST, allowing to be dispersed in an organic solvent or enabling the recyclability of the material by temperature control. Indeed, apart from magnetic nanoparticles, this thermo-responsive polymer can be linked to a variety of noble metal (e.g. Au, Ag or Cu) for sensing and catalytic applications [22], or as was mentioned, with magnetic NPs (e.g. iron oxide NPs) [23,24], thus improving their individual properties when they are located together in the same area [25–27]. It is important to mention that apart from the possibility to increase the drug concentration in the desired area using an external magnetic field, for hybrid systems containing magnetic NPs, the application of an alternating magnetic field (AMF) considerably reduces the tumour volume through magnetic hyperthermia. In fact, 5FU, cisplatin or doxorubicin, which have some limitations in terms of unspecific toxicity, have been accumulated into pNIPAM nanoformulations to enhance their anticancer performance and reduce some side effects [20,28,29]. More recently, Kim et al. fabricated a thermo-responsive pNIPAM hydrogel containing magnetite NPs with allylamine as comonomer to incorporate folic acid as targeting ligand for cervical cancer cell lines [30]. Shen et al. synthesised a pNIPAM thermo-responsive drug release system with encapsulated Fe_3O_4 magnetic NPs and 5FU. In this system, mesoporous SiO_2 was used as the channel for drug release, which enhanced the drug loading rate [31]. Li et al. reported on a successful preparation of a dual-responsive polymer carrier with a magnetic core using N,N-bis(acryloyl)cystamine as a crosslinker [32]. Apart from the phase transition at $32\,^\circ$C, these systems suffered biodegradation of the polymer capsule by cleavage of the disulphide bonds within the cross-linker in the presence of glutathione for hydrophobic and hydrophilic drug release.

In this work, we present a detailed investigation concerning the synthesis, characterisation of a series of hybrid microgel systems composed by magnetic NPs encapsulated by pNIPAM. These colloidal systems were investigated for the accumulation and controlled release of two chemotherapeutic drugs, 5FU and OXA. The synthesis of hybrid microgels was performed at several cross-linker densities and by using different monomer concentrations, as well as in presence of allylamide (AL) as comonomer to covalently incorporate FITC molecules into the microgel network. As mentioned, the fabrication of hybrid materials formed by magnetic nanoparticles and pNIPAM has been previously reported. However, there is a lack of an exhaustive study concerning the control in microgel the dimension as well as the influence of the cross-linker density. The principal novelty in our work is that we have included a detailed investigation concerning the synthesis of pNIPAM@Fe_3O_4 microgels using different monomer concentration as well as several cross-linker densities. We also include encapsulation efficiencies and drug delivery values for 5FU and OXA as model chemotherapeutic drugs. We finally performed cytotoxicity and biocompatibility assays, as well as cell migration studies, which were performed under the application of an external magnetic field. The morphology as well as the hybrid magnetic structure was confirmed by TEM analysis. Particle dimension (hydrodynamic diameter) in function of temperature was monitored by DLS measurements. The presented *in vitro* cytotoxicity investigations

Table 1. pNIPAM radical polymerisation conditions.

	N-Isopropylacrylamide (NIPAM)			N,N′-Methylenbisacrylamide (BIS)		
Entry	g	mmol	mM	g	mmol	%
1	0.113	1.0	50	0.015	0.10	10
2	0.170	1.5	75	0.023	0.15	10
3	0.226	2.0	100	0.031	0.20	10
4	0.339	3.0	150	0	0	0
5	0.339	3.0	150	0.015	0.075	2.5
6	0.339	3.0	150	0.023	0.15	5
7	0.339	3.0	150	0.032	0.21	7.5
8	0.339	3.0	150	0.046	0.30	10
9	0.453	4.0	200	0.062	0.40	10
10	0.566	5.0	250	0.077	0.50	10

reveal that the hybrid magnetic microgels are not toxic and appear to be a great promise to be used in controlled drug delivery and tumour targeting toxicity for biomedical applications by exploiting their magnetic response.

Materials and methods

Materials

N-Isopropylacrylamide (NIPAM), 3-butenoic acid (3BA), acrylic acid (AA), allylamine (AL), fluorescein isothiocyanate isomer I (FITC), 5-fluorouracil (5FU), oxaliplatin (OXA), N,N′-methylenebisacrylamide (BIS), and 2,2′-azobis(2-methylpropionamidene) (V50) were supplied by Aldrich. All reagents were used without further purification. Water was purified using a Milli-Q system (Millipore).

Characterisation

UV–vis spectra were recorded with an Agilent 8453 UV-vis spectrophotometer using a 1 cm quartz cell. DLS measurements were carried out in a Zetasizer Nano S from Malvern Instruments, at a detection angle of $\theta = 173°$ and at a scattering q vector $q = 0.0264\,nm^{-1}$. For TEM imaging a JEOL JEM1400 TEM microscope operated at 100 kV was employed. 10 μL of each colloidal solution were dropped on 100 mesh copper TEM grids and left to dry. The Raman spectra were acquired using a near-infrared (NIR) diode laser at 785 nm (Renishaw inVia Raman spectroscope). A small portion of pNIPAM systems sample was placed on a glass slide. Adsorption analyses were carried out in a XGT-5000WR (Horiba) spectrometer.

Preparation of pNIPAM nanoparticles (pNIPAM@)

The polymerisation reaction was carried out under Ar atmosphere in a three-neck round bottom flask (25 ml) by mixing N-isopropylacrylamide (NIPAM, see Table 1) and N,N′-methylenbisacrylamide (BIS, 10% mmol) in degassed H_2O (Ar, 20 ml) at 70 °C under medium magnetic stirring. A homogeneous mixture was observed when the reaction temperature was reached (∼10 min). Then, 2,2′-azobis(2-methylpropionamidene) (V50, 100 mM, 0.150 ml) was added as radical initiator. After 10 min, the reaction medium became turbid, meaning a successful polymerisation. Then, the flask was sealed and the mixture was maintained at 70 °C for 2 h. After this period of

time, the mixture was allowed to cool down at room temperature under stirring and then it was transferred to centrifuge tubes and centrifuged at 8000 rpm for 1 h. After that, the supernatant was removed and the pellet was redispersed in H_2O (20 ml) to produce a clear colloidal dispersion. This centrifugation process was repeated 4 times. An aliquot was taken and lyophilised for analyses. This sample was kept at 5 °C and protected from light.

Preparation of pNIPAM-co-3BA@, pNIPAM-co-AA@ and pNIPAM-co-AL@ co-polymeric nanoparticles

Co-polymeric nanoparticles were prepared by mixing the monomer N-isopropylacrylamide (3 mmol, 0.339 g) and the cross-linker N,N′-methylenbisacrylamide (0.3 mmol, 0.046 g) in MilliQ H_2O (20 ml). Here, when the reaction temperature was reached (70 °C), the co-monomer (3BA, 0.35 mmol, 0.03 g, 0.03 ml, or AA, 1.51 mmol, 0.021 g, 0.020 ml, or AL, 50 mM, 1 ml) and the radical initiator V50 (100 mM, 0.150 ml) were sequentially added. The purification of nanoparticles was carried out as in the previous case.

Preparation of magnetic (@Fe$_3$O$_4$) nanoparticles by the co-precipitation method

In a three-neck round bottom flask (50 ml), a mixture of tetramethylammonium hydroxide (TMAOH, 25%wt in MeOH, 10.5 ml, or 25% wt, 10.5 ml) and MilliQ H_2O (22 ml) was stirred at 70 °C. Then, a solution of $FeCl_3·6H_2O$ (4 mmol, 1083 mg) and $FeCl_2$ (1.97 mmol, 250 mg) in MilliQ H_2O (3 ml) was added dropwise. After the addition, a dark black precipitated was observed at the bottom of the flask. Then, the reaction mixture was stirred for 30 min at 70 °C. After that, the mixture was allowed to cool down at room temperature, and in order to remove the excess of TMAOH, magnetic decantation (neodimiun magnet) was carried out. Decantation was not observed when water was used as a solvent, then nanoparticles were isolated by centrifugation (8000 rpm, 1 h). In all cases, the supernatant was discarded and the precipitated was washed with MilliQ H_2O (3 × 10 ml) [24]. An aliquot of the dispersion (1 ml) was used to calculate the dry residue, which was obtained by introducing the sample in an oven at 80 °C during 12 h. Co-precipitation was also carried out by using NaOH in water (0.4 M, 20 ml) [33].

Functionalization of magnetic nanoparticles with 3-butenoic acid (@Fe$_3$O$_4$-3BA) or acrylic acid (@Fe$_3$O$_4$-AA)

In a three-neck round bottom flask (250 ml), the acid derivative (3BA: 9.4 mmol, 0.81 g, 0.8 ml, or AA: 9.4 mmol, 0.678 g, 0.645 ml) was added to a magnetic NPs solution (7.2 mg) in water (100 ml) at room temperature. In order to avoid particle aggregation, the mixture was heated at 70 °C and sonicated for 1 h and then it was allowed to cool down at room temperature. Finally, hexadecyl trimethyl ammonium bromide (CTAB, 200 mM, 2 ml) was added to increase particle stability, and the mixture was stirred for 5 min more. After this period of time, the NPs dispersion was centrifuged (1 h, 8000 rpm),

Table 2. pNIPAM systems encapsulation efficiency (EE%) for oxaliplatin (OXA) and 5-fluorouracil (5FU).

Entry	Drug (mg)	pNIPAM precursor (mg)	pNIPAM system	EE%
1	5FU (20)	10	pNIPAM@+5FU	36.3
2	5FU (20)	10	pNIPAM@Fe$_3$O$_4$-3BA + 5FU	60.7
3	5FU (3)	6	pNIPAM-co-AL-FITC@Fe$_3$O$_4$-AA + 5FU	60.0
4	5FU (6)	17	pNIPAM-co-AL@Fe$_3$O$_4$-AA + 5FU	65.0
5	OXA (10)	10	pNIPAM@+OXA	38.5
6	OXA (10)	10	pNIPAM@Fe$_3$O$_4$-3BA + OXA	77.5
7	OXA (10)	10	pNIPAM-co-AL@Fe$_3$O$_4$-AA + OXA	73.5

the supernatant was removed and the pellet was redispersed in MilliQ H$_2$O (100 ml) containing CTAB (5 mM, 1.25 ml).

Preparation of hybrid pNIPAM magnetic systems: pNIPAM@Fe$_3$O$_4$-3BA, pNIPAM@Fe$_3$O$_4$-AA and pNIPAM-co-AL@Fe$_3$O$_4$-AA

These hybrid colloidal structures were fabricated by using the previously synthesised @Fe$_3$O$_4$-3BA and @Fe$_3$O$_4$-AA nanoparticles as seeds during pNIPAM polymerisation. In a three-neck round bottom flask (25 ml), a monomer mixture of N-isopropylacrylamide (3 mmol, 0.339 g) and N,N-methylenbisacrylamide (0.3 mmol, 0.046 g) were added at room temperature to a @Fe$_3$O$_4$-3BA or @Fe$_3$O$_4$-AA NP dispersion (20 ml) in MilliQ water (20 ml). Then, the mixture was heated at 70 °C and degassed with a flux of Ar for 10 min. Then, V50 (100 mM, 0.150 ml) was added to initiate the polymerisation. For pNIPAM-co-AL@Fe$_3$O$_4$-AA system, allylamine (50 mM, 1 ml) was added at this moment. After the sample became turbid (approx. 10 min), the flask was sealed and the reaction was maintained at 70 °C for 2 h. After that, the mixture was allowed to cool down at room temperature and magnetic decantation (neodimiun magnet) was carried out to remove free pNIPAM microgels. The supernatant was discarded and the precipitated was washed with MilliQ H$_2$O (3 × 20 ml). The magnetic systems were lyophilised and kept at 5 °C and protected from light.

Incorporation of FITC fluorescent marker to pNIPAM-co-AL@Fe$_3$O$_4$-AA nanoparticles

In a round bottom flask (10 ml), FITC (2 mg) was added to a pNIPAM-co-AL@Fe$_3$O$_4$-AA dispersion (4.8 mg) in ethanol (4.8 ml). The reaction mixture was stirred at 20 °C for 24 h and protected from light [34]. After that, the mixture was centrifuged (40 min, 8000 rpm), the supernatant was removed and the pellet washed with MilliQ H$_2$O (4 ml, centrifuged). This process was repeated three times, and finally, the pellet was redispersed in MilliQ H$_2$O (4 ml). This sample was denoted as pNIPAM-co-AL-FITC@Fe$_3$O$_4$-AA

Drug encapsulation into pNIPAM systems: 5-fluorouracil and oxaliplatin

In a typical procedure, a certain amount of drug was added to the previously fabricated pNIPAM-derivative systems (see Table 2) in MilliQ water (10 ml). The mixture was stirred for 48 h at 20 °C. After that, the NPs dispersion was centrifuged (8000 rpm, 1 h), the supernatant was removed and the pellet

containing NPs was redispersed in water (10 ml). The encapsulation efficiency (EE%) was determined by UV spectrophotometry.

In vitro drug release

A sample of lyophilised NPs loading the drug (3 mg of the pNIPAM-derivative system) was suspended in PBS (10 ml). The emulsion was introduced into a cellulose dialysis bag and dialysed against PBS buffer solution of pH 7.4 (50 ml) as stationary phase. Drug release analyses were carried out at 4, 20 and 40 °C to observe the influence of temperature. A PBS aliquot of 3 ml was taken each 10 min during the first 60 min, and every 12 h for a 48 h period. After every extraction, 3 ml of PBS were replaced to keep the same volume. Extracted samples were analysed by UV spectrophotometry (257 nm for 5FU and 248 nm for OXA). Calibration curves were prepared for both drugs.

Proliferation assay

The different nanoformulations of pNIPAM were tested in T84 colon cancer cells to determine their cytotoxicity. Cells were seeded in 48-well plates at a density of 5×10^3 cells/well for 72 h in a range of 1–150 μg/mL of pNIPAM. The cell line was cultured in Dulbecco's Modified Eagle's Medium (DMEM) supplemented with 10% foetal bovine serum (FBS) and a mix of antibiotics in a final concentration of 1% penicillin-streptomycin) (Sigma-Aldrich) and maintained at 37 °C and 5% CO$_2$ in a humidified incubator. The cell viability was determined by the colorimetric assay of Sulforhodamine B (SRB) following the protocol established previously [35].
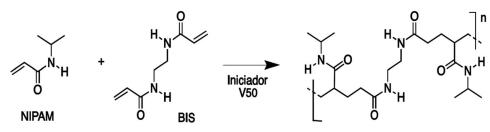
Hemocompatibility assays

Haemolysis and peripheral lymphocytes proliferation assays were carried out to determine pNIPAM nanoformulation hemocompatibility following our protocols reported by Jiménez-López et al. [36]. The lymphocytes viability was determined by Cell Counting Kit-8 (CCK-8) (Dojindo Laboratories, Kumamoto, Japan). The haemolysis percentage was calculated using the following formula:

$$\%HR = \frac{Abs(sample) - Abs(-control)}{Abs(+control) - Abs(-control)} \times 100$$

Application of magnetic fields in vitro

HCT15 cells were seeded in 6-well plates at a cell density of 4×10^5 cells/well and after 24 h of incubation, cells were

Scheme 1. Schematic representation for the pNIPAM polymerisation.

treated with magnetic pNIPAM magnetic nanoformulation (10 μg/mL Fe). After 24 h with the treatment, the medium was discarded, and the cells were washed and trypsinized. Once the cells were centrifuged, they were reseeded in 35 mm Petri dishes and placed over a magnet until the next day. After the incubation time, the cells were fixed and stained following the Sulforhodamine B method referred in the previous section. Finally, plates were photographed to observe the migration of the cells in suspension.

Results and discussion

pNIPAM@ systems

The polymerisation reaction of NIPAM (Scheme 1) has been carried out under free-radical conditions, using an amidinopropane (V50) as initiator and *N,N*-methylenbisacrylamide (BIS) as cross-linker. In order to optimise several parameters as particles size, monodispersity and stability, initially, the polymerisation reaction was performed at several monomer concentrations, from 50 to 250 mM, while the cross-linker BIS molar percentage was changed in the range from 0 to 10% with respect to monomer (Table 1). The radical initiator was used in constant concentration (100 mM) in all cases.

When a monomer concentration of 150 mM and 5% of cross-linker was used, we observed low particle aggregation and high monodispersity (Table 1, entry 6). Samples were analysed by TEM showing sizes in the range of 490 ± 3.0 nm and 530 ± 5.5 nm (Figure 1a). However, when a higher monomer concentration was used (Table 1, entries 9 and 10), important aggregation was observed, which was not improved by reducing the cross-linker concentration (Table 1, entry 7). By the other hand, low yields in NPs were observed with a lower monomer concentration, and keeping constant (10%) the BIS concentration (Table 1, entries 1–3); indeed, any attempt to improve the sample monodispersity by adding lower cross-linker concentrations was unsuccessful (Table 1, entries 4 and 5).

As was detailed in the experimental section, the synthesis of co-polymeric NPs was achieved by using 3-butenoic acid, acrylic acid and allylamine as co-monomers. Particle preparation was carried out by following the optimal conditions determined for pure pNIPAM NPs (Table 1, entry 6). We have demonstrated the presence of co-monomers into the polymeric network by ZP analysis, showing values at pH = 8 of -16 ± 0.305 mV and -14 ± 0.244 mV for the pNIPAM-co-3BA@ and pNIPAM-co-AA@ systems, respectively, meaning partial deprotonation of carboxylic acid groups into the microgel network. However, ZP values for acidic copolymers

derivatives and pNIPAM in neutral or acidic conditions were 0 mV. ZP value for pNIPAM-co-AL@ NPs was around 7.08 ± 0.63 mV at pH = 2, indicating the protonation of amine groups. Indeed, pNIPAM@ and pNIPAM-co-3BA@ systems were also analysed by Raman spectroscopy to confirm their chemical composition (Supplementary Figure 1). pNIPAM@ systems show bands at 442, 845, 1162 and 1457 cm^{-1} that can be assigned to pNIPAM vibrations, while 3BA modified structures show the non-overlapping 3-butenoic acid bands at 153, 603 and 790 cm^{-1}. TEM analysis of pNIPAM and co-polymeric microgel (Figure 1) showed that the particle morphology was not affected by the chemical composition. A low polydispersity was measured with sizes between 519 ± 3.0 nm and 540 ± 5.5 nm for pNIPAM@3-BA particles.

Magnetic pNIPAM systems

As was mentioned, magnetic NPs (@Fe$_3$O$_4$) were prepared by the co-precipitation method in water using TMAOH 25% (in water or methanol) or NaOH as bases. In all cases, the quantity of Fe$_3$O$_4$ was measured by weight determination of solid residue, showing the presence magnetite in 7.2 mg/mL when the synthesis was performed with TMAOH in methanol, and 8.66 mg/mL when TMAOH in water was used. However, when NaOH was added as a base for particle preparation, the solid residue was only 4 mg/mL. These results confirm a more effective process when TMAOH in water was used. In order to incorporate a terminal double bond on the particle surface, magnetite NPs were treated with AA and 3-BA (Figure 2). This process was carried out under heating and sonication in order to avoid particle aggregation. It is important to remark that this functionalization step only slightly affects to the particle size, DLS measurements of magnetite NPs functionalised with 3-BA acid showed a size of 144.3 nm ± 7.9, while magnetic NPs modified with AA presented smaller but similar diameter (140.3 nm ± 8.0). This particle size fits with those previously reported by Laurenti et al. [24] where the size of the magnetite clusters in Fe$_3$O$_4$ NPs decreased with the amount of 3-BA added during particle functionalization.

As was detailed in the experimental section, a pNIPAM and pNIPAM-co-AL polymeric shells were grown by using the @Fe$_3$O$_4$-AA and the @Fe$_3$O$_4$-3BA systems as seeds. ZP values for the hybrid systems structured as a magnetic core surrounded by a polymeric shell were in the order of -14 ± 0.3 mV for pNIPAM@Fe$_3$O$_4$-3BA and pNIPAM@Fe$_3$O$_4$-AA (measured at pH = 8), which can be associated to the presence of deprotonated carboxylic acids. Interestingly, ZP values were -11 ± 0.3 mV at pH = 8 and 2.03 ± 0.6 mV at pH = 2 for co-polymeric (pNIPAM-co-AL) system. These values are

pNIPAM

pNIPAM-co-3BA

a)

2.0 µm

b)

1.0 µm

c)

0.5 µm

d)

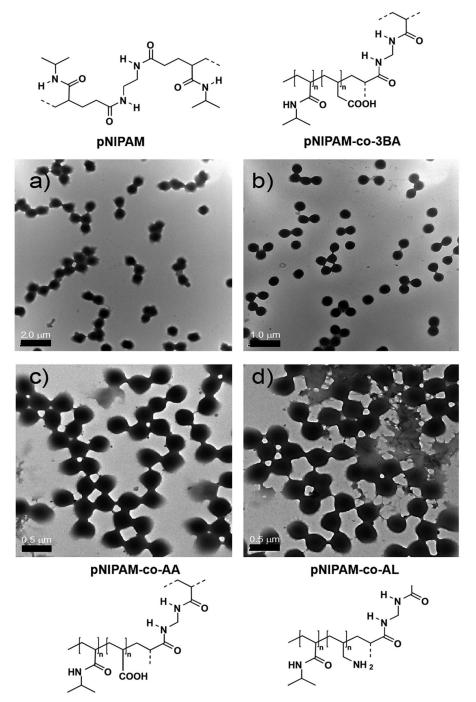0.5 µm

pNIPAM-co-AA

pNIPAM-co-AL

Figure 1. TEM micrographs and chemical structures of (a) pNIPAM@ NPs (monomer concentration 150 mM and 5% BIS) and the co-polymeric systems: (b) pNIPAM-co-3BA@ (c) pNIPAM-co-AA@, and (d) pNIPAM-coAL@.

consistent with particle chemical composition as well as for the data obtained above for the solid pNIPAM NPs. In order to vary the final particle size, we have also performed the pNIPAM polymerisation on the @Fe$_3$O$_4$-AA and @Fe$_3$O$_4$-3BA NPs at several monomer concentrations (50, 75, 150 and 200 mM), all of them at 10% BIS. Figure 3 represents TEM images of the pNIPAM@Fe$_3$O$_4$-3BA hybrid particles at several cross-linker densities. As in the previous case for pure pNIPAM microgels, at a monomer concentration of 50 mM the smallest microgels were obtained. A high contrast cluster of oxide metal spheres coated by a low contrast mono-dispersed polymer shell is shown. In most of the cases,

magnetic clusters are coated by a spherical polymer, however, there is an important presence of non-coated free magnetite aggregates, and some magnetic clusters are coated by a non-defined or irregular polymer shell (Figure 3(a)). At a NIPAM concentration of 75 mM (Figure 3(b)), the number of free non-coated magnetite aggregates is reduced, compared with the sample at 50 mM. However, the amount of non-defined or irregular microgels surrounding the magnetic cluster increases. Importantly, at 150 mM and 200 mM of NIPAM the free non-coated magnetite aggregates almost disappeared, probably due to the higher amount of monomers, however, the magnetite clusters are fully coated by non-
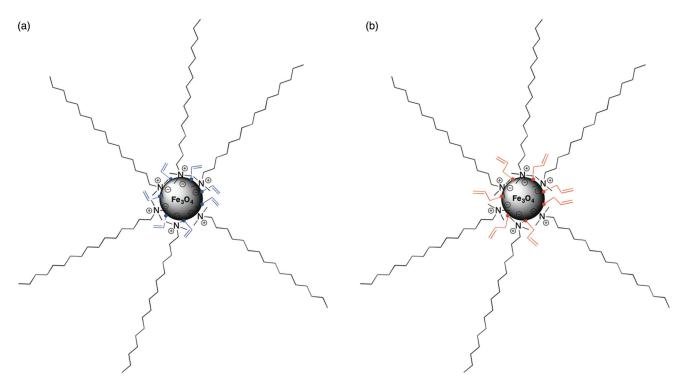
(a)

(b)

Figure 2. Schematic representation of surface modification of magnetic NPs: (a) acrylic acid (@Fe3O4-AA) and (b) 3-butenoic acid (@Fe$_3$O$_4$-3BA).
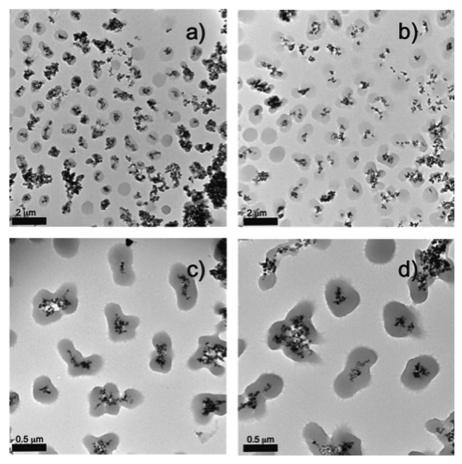

Figure 3. TEM images of pNIPAM@Fe$_3$O$_4$-3BA samples prepared with different monomer concentrations (a) 50, (b) 75, (c) 150 and (d) 200 mM.

defined or irregular microgels. Some of these core@shell particles seem as two fused pNIPAM microgels with the magnetic cluster in the centre (Figure 3(c,d)). Based on these results, we consider 50 mM as optimal NIPAM concentration to obtain magnetic NPs coated by spherical pNIPAM microgels. Therefore, we have analysed the effect of different
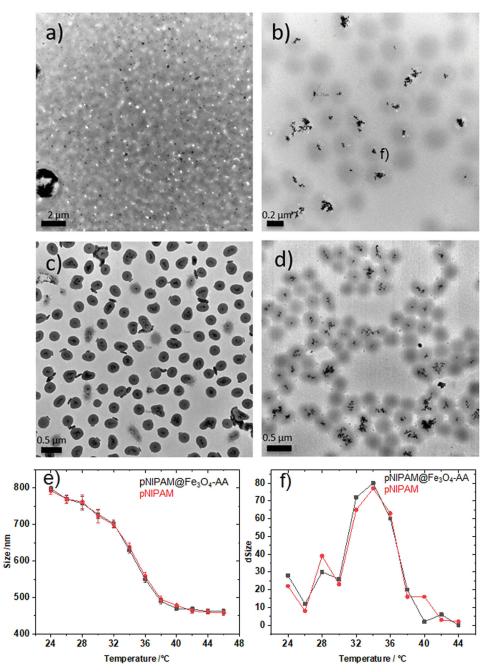
Figure 4. TEM images of pNIPAM@Fe$_3$O$_4$-AA prepared at different cross-linker percentages: (a) 0, (b) 2.5, (c) 5 and (d) 7%; (e) hydrodynamic diameter of the pNIPAM@Fe$_3$O$_4$-AA (black line) and pure pNIPAM (red line) microgels in function of temperature; (f) change of particle size in function of temperature for pNIPAM@Fe$_3$O$_4$-AA (black line) and pure pNIPAM (red line) microgels. The coalescence temperature is 34 °C in both cases.

cross-linker concentrations during the preparation of hybrid magnetic systems at NIPAM monomer concentration of 50 mM.

Figure 4 includes TEM images for pNIPAM@Fe$_3$O$_4$-AA at 0, 2.5, 5 and 7% BA. As is observed, at 0% cross-linker, there is a total absence of microgels, the hybrid core@shell structure was totally lost, a continuous network containing well-dispersed Fe$_3$O$_4$ NPs was observed on the TEM grid (Figure 4(a)). The sample prepared at 2% BIS (Figure 4(b)) resulted in hybrid core@shell systems containing magnetite clusters coated by spherical microgels but with a low number of magnetic NPs within each microgel, and high amount of free microgels, thus reducing the magnetic response. On the contrary, the sample prepared at 7% BIS presented hybrid

systems containing magnetic clusters with an irregular number of magnetite NPs (Figure 4(d)). However, for the hybrid system prepared at 5% BIS homogeneous cores containing magnetic clusters with a regular and constant number of magnetite NPs and well-coated by a spherical microgel was obtained (Figure 4(c)). These data also confirm that the presence of the magnetic core does not affect the polymerisation reaction process. It is also influenced by the amount of monomer and cross-linker. After obtaining the optimal conditions for the fabrication of well-defined core@shell pNIPAM@Fe$_3$O$_4$-AA particles we have determine their size and monodispersity. The measured average size was 260 ± nm. We have determined the low critical solution temperature (LCST) for hybrid magnetic systems (pNIPAM@Fe$_3$O$_4$-AA)

prepared by using 50 mM of monomer and 5% of cross-linker concentrations, as optimal conditions. Figure 4(e) includes Dh measurements taken every 2 °C in a temperature interval from 24 °C (590 nm) to 46 °C (252.5 nm) where the two microgel states (swollen and collapsed) are easily observed. Figure 4(f) shows the change of the particle size in function of temperature, the maximum value indicates the LCST, which can be established at 34 °C. As can be observed, the hydrodynamic diameter in the function of temperature for pNIPAM@Fe$_3$O$_4$-AA systems (black line) fits with the hydrodynamic diameter for pure pNIPAM microgles (red line). Indeed, the LCST is produced at 34 °C in both cases. These data support that the presence of the magnetic core does not influence the final particles size and temperature behaviour of pNIPAM microgel.

The final particle size below the LCST depends on the cross-linker amount into the microgel network. This dependence can be extracted from Flory's theory [37], which establishes that in a microgel, the macroscopic swelling-deswelling behaviour is determined by the balance of mixture, elastic and ionic osmotic components. Therefore, a polymer with a low cross-linker density has a more intense phase transition due to a lower elastic component. However, above the LCST pNIPAM is totally collapsed because water molecules are expelled from the microgel network. Consequently, we have analysed the Dh values for pNIPAM@Fe$_3$O$_4$-AA particles at 24 and 46 °C and at four different cross-linker densities (0, 2.5, 5 and 7%). In this situation the measured hydrodynamic diameters were 148, 668, 590 and 500 for 0, 2.5, 5 and 7%, respectively at 24 °C and similar in all cases at 46 °C (∼250 nm), and aggregation was not observed.

Finally, we have measured Fe contents by atomic absorption technique in pNIPAM@Fe$_3$O$_4$-3BA and pNIPAM@Fe$_3$O$_4$-AA systems with 150 mM NIPAM and 5% BIS, which were quantified in 205 mg/g and 198 mg/g of NPs (RSD 3.8%), respectively. We have also mentioned that co-polymeric NPs (pNIPAM-co-AL@Fe$_3$O$_4$-AA) were prepared by polymerisation of NIPAM (50 mM), BIS (5%) and allylamine in the presence of @Fe$_3$O$_4$-AA magnetic cores. Figure 5(a) and b show TEM images at different a magnification of the hybrid pNIPAM-co-AL@Fe$_3$O$_4$-AA NPs. Again, well-dispersed spherical microgels containing magnetic clusters with Fe$_3$O$_4$ aggregates are observed. This system was designed for the incorporation of the chromophore FITC, by a reaction of the free amine group present into the polymer network (provided by allylamine) with the isothiocianate group from FITC, as is represented in Figure 5(c). The reaction proceeded under smooth conditions, and incorporation of chromophore was achieved quantitatively to obtain the pNIPAM-co-AL-FITC@Fe$_3$O$_4$-AA system. The presence of FITC in the hybrid systems was confirmed by confocal microscopy (Figure 5(d,e)).

Encapsulation of 5-fluorouracil and oxaliplatin

Encapsulation of 5FU was carried out in pNIPAM@, pNIPAM@Fe$_3$O$_4$-3BA and pNIPAM-co-AL@Fe$_3$O$_4$-AA systems, while OXA was only included into pNIPAM@ and pNIPAM@Fe$_3$O$_4$-3BA particles. The drug loading was carried out at 20 °C due at this temperature the pNIPAM network is

expanded. Drug loading was achieved by adding from 3 to 20 mg of the active compound to a water dispersion of pNIPAM@ systems (Table 2). The drug encapsulation efficiency (EE%) into polymeric systems was monitored by UV spectrophotometry on centrifuged samples measuring the UV absorption at 257 and 248 nm, for 5FU and OXA, respectively [30]:

$$EE\% = \frac{D_L - D_F}{D_F} \cdot 100$$

where D_L is the initial added concentration of drug and D_F is the concentration of the free drug after centrifugation. Results are shown in Table 2 as an average of two measurements.

As can be extracted from Table 2, good encapsulation efficiencies was obtained in all cases. It is worth to note that EE% for magnetic NPs were higher (Table 2, entries 2–4, 6, and 7) than that for pure NIPAM@ systems (Table 2, entries 1 and 5), being a constant effect for all the prepared systems. We attribute this effect to the higher expanded size (up to 800 nm) of hybrid systems, allowing the accumulation of the drug in a higher solution volume. On the other hand, better entrapment efficiencies were obtained for OXA (up to 77.5%, Table 2, entry 6) than for 5FU (65.0% maximum, Table 2, entry 4), this fact can be attributed to a better water solubility of 5FU, increasing its tendency to stay in aqueous solution.

In vitro 5-fluorouracil and oxaliplatin release

In vitro release of 5FU and OXA was studied by using a cellulose dialysis bag placed in an Erlenmeyer containing PBS buffer solution at pH = 7.4, as stationary phase and at constant stirring of 100 rpm. At intervals of 10 min during the first 60 min and every 12 h for a 48 h period, aliquots of 3 ml were withdrawn from the solution. The release medium was replaced with the same volume of PBS. Analyses were carried out at several temperatures (4, 20 and 40 °C) to observe the influence of temperature in drug delivery (Figure 6). Drug release was measured by UV spectrophotometry (257 nm for 5FU and 248 nm for OXA). Figure 6 shows drug delivery results for pNIPAM@+5FU and pNIPAM-co-AL@Fe$_3$O$_4$-AA + OXA. As can be observed, only at about 2.5% of cumulative drug release has been reached at 4 °C and at 20 °C, for both drugs, meaning that the drug is strongly retained inside of the swollen polymer matrix. However, at 40 °C the percentage of release is almost 42% along the first 60 min, reaching 81% after 48 h due to the microgel collapse.

Cytotoxicity and biocompatibility of blank nanoparticles

As shown in Figure 7, pNIPAM blank nanoformulations showed no cytotoxicity in the T84 human colon cancer cell line. Only pNIPAM@Fe$_3$O$_4$-3BA was slight cytotoxic from the 10 μg/mL of pNIPAM dose showing a small viability decrease (∼93%) (Figure 7). In addition, the nanoformulation biocompatibility was tested in blood cells where blank pNIPAM@ and pNIPAM@Fe$_3$O$_4$-3BA did not produce any erythrocyte
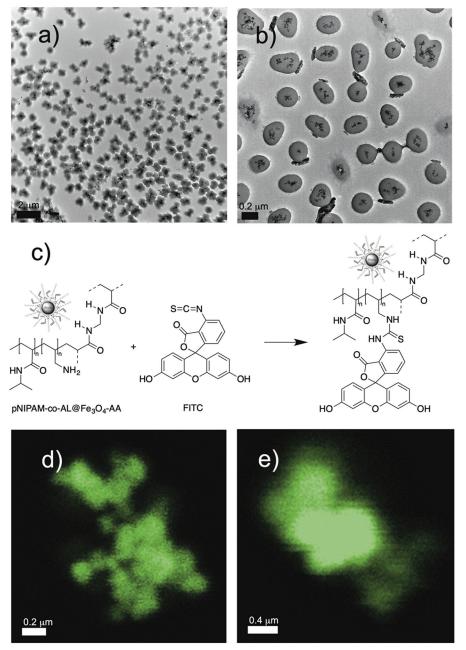
Figure 5. TEM micrographs of pNIPAM-co-AL@Fe₃O₄-AA NPs (a,b); introduction of FITC (c); and confocal images (d and e) of pNIPAM-co-AL-FITC@Fe₃O₄-AA.
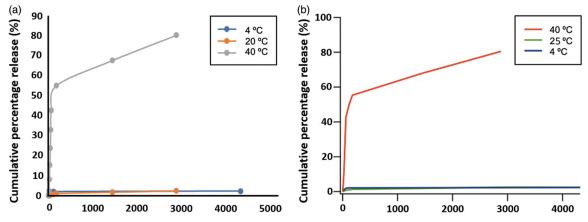

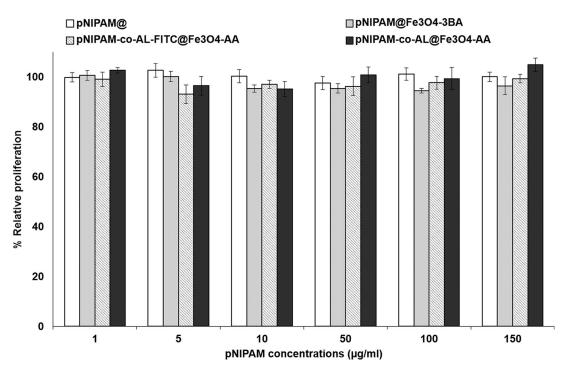**Figure 6.** Drug release. pNIPAM@+5FU (a) and pNIPAM@Fe₃O₄-AA + OXA (b) cumulative drug release.

Figure 7. Cytotoxicity assay of blank pNIPAM@ nanoformulations in T84 colon cancer cell line. Results are expressed as the mean ± SD and the experiment was made in triplicate cultures.
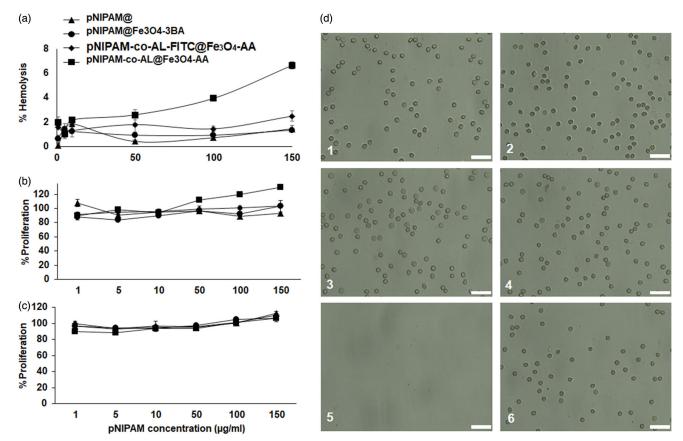

Figure 8. Blood biocompatibility assays. Haemolysis assay with red blood cells (a). CCK-8 test on peripheral blood lymphocytes at 1 h (b) and 12 h of exposition (c). Light microscopy images of human erythrocytes after 1 h of treatment with a pNIPAM@ (d1), pNIPAM@Fe₃O₄-3BA (d2), pNIPAM-co-AL-FITC@Fe₃O₄-AA (d3), pNIPAM-co-AL@Fe₃O₄-AA (d4), at a dose of 150 μg/mL. The images (d5) and (d6) are positive and negative control respectively. Scale bar 25 μm.

lysis even at the highest concentrations tested (150 μg/mL of pNIPAM) (Figure 8(a)). Only pNIPAM-co-AL@Fe₃O₄-AA showed a slight haemolysis increase at the highest doses. Moreover, no agglutination of erythrocytes was observed in any of the nanoformulations tested after 1 h of exposure (Figure 8(d)). Finally, pNIPAM blank nanoformulations neither produced toxicity in white blood cells at any of the tested doses after 1 (Figure 8(b)) and 12 h (Figure 8(c)) of exposure. Only a slight
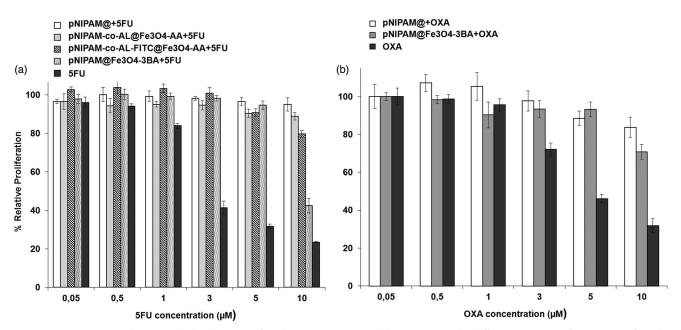
Figure 9. Cytotoxicity assay with pNIPAM-loading drugs nanoformulations. T84 tumour cell line was exposed to different treatments of pNIPAM nanoformulations loaded with 5FU (a) and with OXA (b) compared to their respective free drugs. Results are expressed as the mean ± SD and the experiment was made in triplicate cultures.

white blood cell overgrowth was detected at the pNIPAM-co-AL@Fe$_3$O$_4$-AA high doses after 12 h of exposition. These results suggest that pNIPAM@, pNIPAM@Fe$_3$O$_4$-3BA and pNIPAM-co-AL-FITC@Fe$_3$O$_4$-AA have excellent biocompatibility with human blood cells, an essential characteristic for their *in vivo* use, being a possible antitumor drug vehicle of antitumor drugs for intravenous administration. In fact, previous pNIPAM@ nanoformulations have already been described as therapeutic delivery system [38–40]. Recently, Salimi et al. used a similar system to deliver cisplatin against hepatocarcinoma cells [39]. Interestingly, a slight lymphocytes overgrowth was observed with the use of pNIPAM-co-AL@Fe$_3$O$_4$-AA at 12 h of exposure. This fact could be related to the T lymphocytes capacity to synthesise iron-containing molecules (e.g. transferrin) using the iron of the pNIPAM@ NPs [41]. In fact, other authors demonstrated that the iron NPs administration may modify the behaviour of the immune system inducing the alteration of the lymphocytes levels in blood [42,43].

Proliferation studies of the drugs-loaded pNIPAM@ nanosystems

pNIPAM@ nanoformulations were loaded to 5FU and OXA to determine the modulation of cytotoxic effect against colon cancer cells. Of all the nanoformulations analysed (Figure 9(a)), pNIPAM @ Fe$_3$O$_4$-3BA + 5FU showed the highest cytotoxic effect against T-84 colon cancer cells, with a relative inhibition of proliferation (57%) ($p < .05$) close to that observed with free 5FU. Taking into account the properties of pNIPAM@ which is sensitive to temperature and/or a pH, an improvement in 5FU release could be obtained with modulation of these variables. Interestingly, our studies

demonstrated that a temperature of 40 °C allowed 81% of drug release after 48 h of incubation (Figure 6). This temperature could be obtained by hyperthermia [44]. In fact, Wang et al. increased the curcumin release from carbon NPs (FCNPs) associated with pNIPAM nanogels increasing temperature by the use of near-infrared (NIR) light irradiation [45]. These authors achieved 60% of cell death in the B16F10 melanoma cell line with only 5 min of NIR light exposition. New studies will be necessary to determine the improvement of 5FU from our nanoformulations after changes in temperature. On the other hand, pNIPAM@ nanoformulations can also take advantage of the slightly more acidic pH in the tumours that can stimulate the drug release [46]. Recently, Salimi et al. synthesised a nanogel of pNIPAM and poly(N,N-(dimethylamino)ethyl methacrylate) (P(NIPAM-co-DMA) with dual-responsive (sensitive to temperature and pH) and loaded with cisplatin [39]. This nanoformulation induced a higher cytotoxic effect in HepG2 hepatocellular carcinoma cells than free cisplatin. In our case, despite both pNIPAM@+OXA and pNIPAM@Fe$_3$O$_4$-3BA + OXA showed lower cytotoxicity against T-84 colon cancer than free OXA ($p < .05$) (Figure 9(b)), more assays with modulation of pH and/or temperature will be necessary to determine their antitumor efficacy.

Cell migration under a magnetic field in vitro

Treatment with pNIPAM-co-AL@Fe$_3$O$_4$-AA at a dose of 10 µg/mL of Fe resulted in a slight migration of HCT15 cells in suspension in the presence of an external magnetic field. By contrast, free Fe at the same dose did not produce any cell migration (Figure 10). This could be indicative of the remaining magnetic potential of nanoformulation once they are
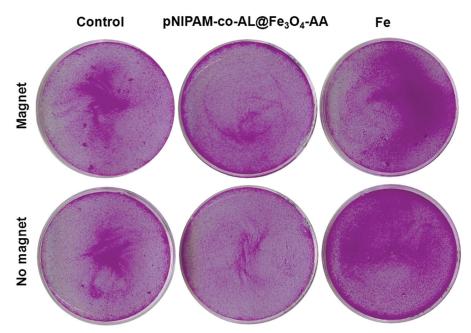
Figure 10. Migration assays using the magnetic pNIPAM-co-AL@Fe$_3$O$_4$-AA nanoformulation. Cells were exposed to 10 μg/mL Fe of pNIPAM-co-AL@Fe$_3$O$_4$-AA and free iron to compare the migration of the detached cells under a magnetic field.

internalised although new complementary studies will be necessary.

Conclusions

In summary, we have synthesised a series of hybrid thermoresponsive microgels containing Fe$_3$O$_4$ NPs for drug loading and release investigations. Initially, we have optimised the monomer concentration and the crosslinker percentage for the fabrication of highly monodisperse and stable free pNIPAM microgels. Then, we have synthesised Fe$_3$O$_4$ NPs by 3 different approaches, thus including TMAOH (in methanol and water) and NaOH as alkaline bases. Fe$_3$O$_4$ NP surface was derivatized to provide a terminal double bond by using 3BA and AA, to be polymerised with pNIPAM by free radical polymerisation, obtaining a hybrid core@shell system in all cases. Several monomer concentration and crosslinker percentage were used in order to optimise size and particle aggregation in both outsides and within the microgel. We have also incorporated allylamine as co-monomer to target FITC. High encapsulation efficiencies were obtained for 5FU and OXA in all cases. Drug release was performed against PBS, obtaining better drug release behaviour above the LCST, as the pNIPAM is in the collapsed state. Importantly, our new pNIPAM nanoformulations showed great biocompatibility, an excellent capacity to load specific drugs against colon cancer cells and high sensitivity to the temperature that allows to increase drug release and to improve cytotoxic therapy in this type of tumour. These results suggest the possible application of combined therapy (5FU and OXA) using a single nanoformulation that could be directed directly to the tumour through an external magnetic field. Thus, the presented hybrid systems possess potential applications in localised drug delivery making it a very promising tool for colon cancer therapy.

Disclosure statement

No potential conflict of interest was reported by the author(s).

Funding

References

[1]   Bray F, Ferlay J, Soerjomataram I, et al. Global cancer statistics 2018: GLOBOCAN estimates of incidence and mortality worldwide for 36 cancers in 185 countries. CA Cancer J Clin. 2018;68(6):394–424.

[2]   NCBI. Colon Cancer Treatment (PDQ®) - PDQ Cancer Information Summaries - NCBI Bookshelf [Internet]. 2019. [cited 2019 Apr 29]. Available from: https://www.ncbi.nlm.nih.gov/books/NBK65858

[3]   Mármol I, Sánchez-de-Diego C, Pradilla Dieste A, et al. Colorectal carcinoma: a general overview and future perspectives in colorectal cancer. Int J Mol Sci. 2017;18:197.

[4]   Ghiringhelli F, Apetoh L. Enhancing the anticancer effects of 5-fluorouracil: current challenges and future perspectives. Biomed J. 2015;38(2):111–116.

[5]   Zhang N, Yin Y, Xu S-J, et al. 5-Fluorouracil: mechanisms of resistance and reversal strategies. Molecules. 2008;13(8):1551–1569.

[6]   André T, Boni C, Mounedji-Boudiaf L, et al. Oxaliplatin, fluorouracil, and leucovorin as adjuvant treatment for colon cancer. N Engl J Med. 2004;350(23):2343–2351.

[7]   Perego P, Robert J. Oxaliplatin in the era of personalized medicine: from mechanistic studies to clinical efficacy. Cancer Chemother Pharmacol. 2016;77(1):5–18.

[8]   Casale F, Canaparo R, Serpe L, et al. Plasma concentrations of 5-fluorouracil and its metabolites in colon cancer patients. Pharmacol Res. 2004;50(2):173–179.

[9] Griffith KA, Zhu S, Johantgen M, et al. Oxaliplatin-induced peripheral neuropathy and identification of unique severity groups in colorectal cancer. J Pain Symptom Manage. 2017;54(5): 701–706.e1.

[10] Shi J, Kantoff PW, Wooster R, et al. Cancer nanomedicine: progress, challenges and opportunities. Nat Rev Cancer. 2017;17(1): 20–37.

[11] Schild HG. Poly(N-isopropylacrylamide): experiment, theory and application. Prog Polym Sci. 1992;17(2):163–249.

[12] Sawai T, Yamazaki S, Ikariyama Y, et al. pH-Responsive swelling of the ultrafine microsphere. Macromolecules. 1991;24(8):2117–2118.

[13] Tanaka T, Fillmore D, Sun S-T, et al. Phase transitions in ionic gels. Phys Rev Lett. 1980;45(20):1636–1639.

[14] McPhee W, Tam KC, Pelton R. Poly(N-isopropylacrylamide) latices prepared with sodium dodecyl sulfate. J Colloid Interface Sci. 1993;156(1):24–30.

[15] Suzuki A, Tanaka T. Phase transition in polymer gels induced by visible light. Nature. 1990;346(6282):345–347.

[16] Rejinold NS, Baby T, Chennazhi KP, et al. Dual drug encapsulated thermo-sensitive fibrinogen-graft-poly (N-isopropyl acrylamide) nanogels for breast cancer therapy. Colloids Surf B Biointerfaces. 2014;114:209–217.

[17] Blanco MD, Guerrero S, Benito M, et al. In vitro and in vivo evaluation of a folate-targeted copolymeric submicrohydrogel based on n-isopropylacrylamide as 5-fluorouracil delivery system. Polymers. 2011;3(3):1107–1125.

[18] Li P, Hou X, Qu L, et al. PNIPAM-MAPOSS hybrid hydrogels with excellent swelling behavior and enhanced mechanical performance: preparation and drug release of 5-fluorouracil. Polymers. 2018;10:137.

[19] Patil AS, Gadad AP, Hiremath RD, et al. Biocompatible tumor micro-environment responsive CS-g-PNIPAAm co-polymeric nanoparticles for targeted oxaliplatin delivery. J Polym Res. 2018; 25(3):77.

[20] Peng J, Qi T, Liao J, et al. Controlled release of cisplatin from pH-thermal dual responsive nanogels. Biomaterials. 2013;34(34): 8726–8740.

[21] Patil AS, Gadad AP. Development and evaluation of high oxaliplatin loaded CS-g-PNIPAAm co-polymeric nanoparticles for thermo and pH responsive delivery. IJPER. 2018;52(1):62–70.

[22] Contreras-Cáceres R, Pastoriza-Santos I, Alvarez-Puebla RA, et al. Growing Au/Ag nanoparticles within microgel colloids for improved surface-enhanced Raman scattering detection. Chemistry. 2010;16(31):9462–9467.

[23] Contreras-Cáceres R, Abalde-Cela S, Guardia-Girós P, Fernández-Barbero A, et al. Multifunctional microgel magnetic/optical traps for SERS ultradetection. Langmuir. 2011;27(8):4520–4525.

[24] Laurenti M, Guardia P, Contreras-Cáceres R, et al. Synthesis of thermosensitive microgels with a tunable magnetic core. Langmuir. 2011;27(17):10484–10491.

[25] Jones ST, Walsh-Korb Z, Barrow SJ, et al. The importance of excess poly(N-isopropylacrylamide) for the aggregation of poly(N-isopropylacrylamide)-coated gold nanoparticles. ACS Nano. 2016; 10(3):3158–3165.

[26] Schmaljohann D. Thermo- and pH-responsive polymers in drug delivery. Adv Drug Deliv Rev. 2006;58(15):1655–1670.

[27] Zheng Y, Wang L, Lu L, et al. pH and thermal dual-responsive nanoparticles for controlled drug delivery with high loading content. ACS Omega. 2017;2(7):3399–3405.

[28] Li G, Song S, Zhang T, et al. pH-sensitive polyelectrolyte complex micelles assembled from CS-g-PNIPAM and ALG-g-P(NIPAM-co-NVP) for drug delivery. Int J Biol Macromol. 2013;62:203–210.

[29] Ma X, Liu Q. Preparation of poly(N-isopropylacrylamide)-block-(acrylic acid)-encapsulated proteinaceous microbubbles for delivery of doxorubicin. Colloids Surf B Biointerfaces. 2017;154: 115–122.

[30] Kim H, Jo A, Baek S, et al. Synergistically enhanced selective intracellular uptake of anticancer drug carrier comprising folic acid-conjugated hydrogels containing magnetite nanoparticles. Sci Rep. 2017;7:41090

[31] Shen B, Ma Y, Yu S, et al. Smart multifunctional magnetic nanoparticle-based drug delivery system for cancer thermo-chemotherapy and intracellular imaging. ACS Appl Mater Interfaces. 2016; 8(37):24502–24508.

[32] Li A, Ma H, Feng S, et al. A copolymer capsule with a magnetic core for hydrophilic or hydrophobic drug delivery via thermo-responsive stimuli or carrier biodegradation. RSC Adv. 2016;6(39): 33138–33147.

[33] Shao X, Dai B, Zhang X, et al. Synthesis and microwave absorption properties of magnetite nanoparticles. Nanosci Nanotechnol. 2012;12:1122–1127.

[34] Liu Y, Shi M, Xu M, et al. Multifunctional nanoparticles of Fe(3)O(4)@SiO(2)(FITC)/PAH conjugated the recombinant plasmid of pIRSE2-EGFP/VEGF(165) with dual functions for gene delivery and cellular imaging. Expert Opin Drug Deliv. 2012;9(10): 1197–1207.

[35] Ortiz R, Cabeza L, Arias JL, et al. Poly(butylcyanoacrylate) and poly(ε-caprolactone) nanoparticles loaded with 5-fluorouracil increase the cytotoxic effect of the drug in experimental colon cancer. Aaps J. 2015;17(4):918–929.

[36] Jiménez-López J, El-Hammadi MM, Ortiz R, et al. A novel nanoformulation of PLGA with high non-ionic surfactant content improves in vitro and in vivo PTX activity against lung cancer. Pharmacol Res. 2019;141:451–465.

[37] Flory P. Principles of polymer chemistry. vol. 1. Ithaca (NY): Cornell University Press; 1953.

[38] Ji P, Zhou B, Zhan Y, et al. Multistimulative nanogels with enhanced thermosensitivity for intracellular therapeutic delivery. ACS Appl Mater Interfaces. 2017;9(45):39143–39151.

[39] Salimi F, Dilmaghani KA, Alizadeh E, et al. Enhancing cisplatin delivery to hepatocellular carcinoma HepG2 cells using dual sensitive smart nanocomposite. Artif Cells Nanomedicine Biotechnol. 2018;46(5):949–958.

[40] Wang L, Jang G, Ban DK, et al. Multifunctional stimuli responsive polymer-gated iron and gold-embedded silica nano golf balls: nanoshuttles for targeted on-demand theranostics. Bone Res. 2017;5:17051

[41] Lum JB, Infante AJ, Makker DM, et al. Transferrin synthesis by inducer T lymphocytes. J Clin Invest. 1986;77(3):841–849.

[42] Chen B-A, Jin N, Wang J, et al. The effect of magnetic nanoparticles of Fe(3)O(4) on immune function in normal ICR mice. Int J Nanomedicine. 2010;5:593–599.

[43] Wang J, Chen BJN, Xia G, et al. The changes of T lymphocytes and cytokines in ICR mice fed with Fe_3O_4 magnetic nanoparticles. Int J Nanomedicine. 2011;6:605–610.

[44] Deshpande S, Sharma S, Koul V, et al. Core-shell nanoparticles as an efficient, sustained, and triggered drug-delivery system. ACS Omega. 2017;2(10):6455–6463.

[45] Wang H, Ke F, Mararenko A, et al. Responsive polymer-fluorescent carbon nanoparticle hybrid nanogels for optical temperature sensing, near-infrared light-responsive drug release, and tumor cell imaging. Nanoscale. 2014;6(13):7443–7452.

[46] Feng Y, Li N-X, Yin H-L, et al. Thermo- and pH-responsive, lipid-coated, mesoporous silica nanoparticle-based dual drug delivery system to improve the antitumor effect of hydrophobic drugs. Mol Pharm. 2019;16(1):422–436.